processes

MDPI

Article

Experimental Investigation into Atmospheric Microwave Plasma-Driven Nitrogen Fixation Using Metal–Organic Frameworks

Fang Zheng, Kai Feng, Shaokun Wu and Wei Xiao *

College of Big Data and Information Engineering, Guizhou University, Guiyang 550025, China; 15117522482@163.com (F.Z.); 18212189667@163.com (K.F.); w1450320208@163.com (S.W.)
* Correspondence: wxiao@gzu.edu.cn

Abstract: Microwave plasma-driven nitrogen fixation can occur at atmospheric pressure without complex processing conditions. However, this method still faces the challenge of high energy consumption and low production. Combined plasma–catalyst systems are widely used to increase production and reduce energy consumption in nitrogen fixation. However, the efficacy of currently used catalysts remains limited. In this paper, the metal–organic framework materials (MOFs) copper benzene-1,3,5-tricarboxylate (Cu-BTC) and zeolitic imidazolate framework-8 (ZIF-8) are combined with atmospheric microwave plasma for nitrogen fixation. The experimental results show that they have a better catalytic effect than the ordinary catalyst zeolite socony mobil-5 (ZSM-5). The maximum nitrogen oxide concentration reaches 33,400 ppm, and the lowest energy consumption is 2.05 MJ/mol. Compared to no catalyst, the production of nitrogen oxides (NO_x) can be increased by 17.1%, and the energy consumption can be reduced by 14.6%. The stability test carried out these catalysts demonstrates that they have a stable performance within one hour. To the knowledge of the authors, this is the first effort to study the synergistic effects of atmospheric microwave plasma and MOFs on nitrogen fixation. This study also introduces a potentially eco-friendly approach to nitrogen fixation, characterized by its low energy consumption and emissions.

Keywords: microwave plasma; metal–organic framework materials; nitrogen oxides; synergistic effects

Citation: Zheng, F.; Feng, K.; Wu, S.; Xiao, W. Experimental Investigation into Atmospheric Microwave Plasma-Driven Nitrogen Fixation Using Metal–Organic Frameworks. *Processes* **2024**, *12*, 2633. https://doi.org/10.3390/pr12122633

Academic Editor: Jichang Liu

Received: 17 October 2024
Revised: 10 November 2024
Accepted: 21 November 2024
Published: 22 November 2024

1. Introduction

As one of the fundamental elements in living organisms, nitrogen is essential for both the growth of plants and human activities such as the production of agricultural and chemical materials [1,2]. Nitrogen mostly exists in the form of N_2 in air which cannot be directly absorbed by organisms [3]. In nature, nitrogen can be fixed through microbial action and lightning [4,5]. The nitrogen-containing compounds produced by these two methods cannot meet the needs of human life. The Haber–Bosch (H-B) process is the most commonly used industrial nitrogen fixation technology, and can supply 40% of the global population with nitrogen demand annually. However, the H-B process heavily relies on fossil energy and causes high CO_2 emissions, exacerbating the greenhouse effect [6,7]. As such, it is necessary to find novel green and sustainable nitrogen fixation technologies.

Recently, the electrochemical process and bionic photocatalytic method have garnered significant attention as green methods for nitrogen fixation. The electrochemical process produces ammonia through the electrocatalytic N_2 reduction reaction (ENRR). Due to the high-energy barrier of N_2 activation and the competing hydrogen evolution reaction, the Faraday efficiency and ammonia yield of the ENRR are significantly constrained [8]. The bionic photocatalytic method leverages visible light to convert N_2 into ammonia using H_2O as a proton source at ambient temperature and pressure. However, the photocatalytic process is hindered by issues such as a low photoelectric conversion efficiency, limited light

absorption range, and low N-N bond dissociation [9], making it challenging to scale up for industrial applications.

Plasma is a quasi-electrically neutral system consisting of electrons, charged ions, and neutral particles, which can provide active species to facilitate difficult chemical reactions [10]. Compared to the H-B process, plasma-based nitrogen fixation can occur in mild conditions, and it has the advantages of a short startup time, fast reaction rate, one-step synthesis, instant control, and suitability for small-scale and decentralized production. Hence, it has gained increasing attention among global scholars. Dielectric barrier discharge (DBD) [11,12], spark discharge [13], gliding arc discharge [14–17], and microwave discharge [18–20] are widely used to synthesize nitrogen oxides in air, and the gliding arc and microwave plasma have the best performance among them. Malik et al. studied nitrogen fixation using the gliding arc; the gas product had no ozone when air was used as the working gas and it achieved an energy consumption of 15.4 MJ/mol and a NO_x yield of 0.1% [17]. A millimeter-scale sliding arc reactor operating at atmospheric pressure was proposed by Patil et al. for the synthesis of NO_x [21]. The energy consumption for NO_x generation was as low as 4.2 MJ/mol, and the NO_x yield was about 1%. Vervloessem et al. proposed a novel atmospheric sliding arc plasma for generating NO_x at different N_2/O_2 gas feed ratios with an energy consumption of 3.6 MJ/mol and a NO_x yield of 1.5% [15]. Kelly and Bogaerts investigated microwave plasma using a vortex gas flow to fix nitrogen from the air into NO_x with the lowest energy consumption recorded of 2 MJ/mol at atmospheric pressure, for a total NO_x yield of 3.8% [20]. Asisov et al. reported the lowest energy consumption of nitrogen fixation, achieved by utilizing low-pressure electron cyclotron resonance (ECR) microwave discharge in N_2/O_2 mixtures in the early 1980s. Notably, they achieved a NO_x production rate of 14% with an energy consumption of only 0.3 MJ/mol [22]. However, their results have never been reproduced up to now. Compared to the H-B process which has an energy consumption of 0.5 MJ/mol [23], it is necessary to study effective means to reduce the energy consumption of the plasma-driven nitrogen fixation.

Catalysts are widely introduced to combine with the plasma to increase NO_x production and decrease the energy consumption of nitrogen fixation [24,25]. The synergistic effects of the plasma and catalysts have been shown in previous studies. Patil et al. added the γ-Al_2O_3 to DBD to fix nitrogen in air with an energy consumption of 18 MJ/mol and a NO_x yield of 0.5%. It was proved that the 5% WO_3/-Al_2O_3 catalyst increased the NO_x yield by about 10% [12]. Xuekai Pei found that the catalyst increased NO_x production even away from the plasma region, which suggested that the catalytic activation of downstream neutrals played an important role [26]. Mutel et al. reported a yield of 6% NO at an energy consumption of 0.84 MJ/mol in microwave plasma at 66 mbar with the MoO_3 catalyst [19]. Baiqiang Zhang et al. proposed a system combining non-thermal plasma and fluidized catalysts with the water vapor as the green feedstock for high-efficiency ammonia synthesis, which reveal that bimetallic Co-Ni-supported catalysts on the MgO carrier exhibit notably higher NH_3 formation rates than single-component metal-supported catalysts and no catalysts [27]. Nguyen Hoang M. reports a novel non-thermal plasma driven N_2 fixation pathway with methane (CH_4) over a low-cost Cu/SiO_2 catalyst to form a high ammonia yield of almost 7%, and the presence of CH_4 promoted the N_2 fixation degree by up to 17% [28]. Metal–organic framework (MOF) catalysts were used in the plasma-driven synthesis of ammonia by Shah et al., who used Ni-MOF-74 as a catalyst for ammonia synthesis in synergy with the radio frequency (RF) plasma which provided a higher ammonia yield of 0.23 g/kWh (on a per-gram-of-catalyst basis) compared to Ni metal [29]. Most of the existing literature on plasma-driven nitrogen fixation combined with catalysts has focused on the use of DBD and RF plasma [29–33]. Microwave plasma has the advantages of being electrode-free, having a high energy efficiency, and a long working life compared with DBD and RF plasmas. Table 1 lists the state-of-the-art investigations into plasma-based nitrogen fixation. The MOF material has advantages over other catalysts, such as a large specific surface area, abundant active sites, and strong adsorption [34].

The typical ZIF series material ZIF-8 has a strong thermal stability, showing a uniform dodecahedral structure under transmission electron microscopy, and it can still maintain a clear dodecahedral structure after undergoing direct carbonization at 1000 °C for 10 h [35]. According to the research by Ahsan Jalal et al., CuBTC, which is a representative of HKUST MOFs, exhibits a strong catalytic performance after being heated at 600 °C for 4 h [36]. And MOFs have been widely studied in the treatment of pesticide residues [37] and heavy metal pollution in water bodies [38], and are environmentally friendly materials. Therefore, the MOF materials CuBTC and ZIF-8 are combined with the atmospheric-pressure microwave plasma for nitrogen fixation in this paper.

Table 1. Plasma-based nitrogen fixation research.

Plasma/Reactor Type	Reactant Gas	NO_x Concentration	Energy Cost (MJ/mol)	Reference
Dielectric Barrier Discharge	N_2, O_2	0.36%	56–140	[11]
Dielectric Barrier Discharge—packed with catalyst	N_2, O_2	0.50%	18	[12]
Spark discharge—pulsed AC	N_2, O_2	0.02%	0.42	[13]
Gliding arc plasmatron	N_2, O_2	1.5%	3.6	[15]
Three-level coupled rotating electrodes plasma	N_2, O_2	0.4–0.5%	2.27–2.8	[16]
Gliding arc plasma	N_2, O_2	0.1%	15.4	[17]
Pulsed microwave discharge	N_2, O_2	7%	8	[18]
Microwave plasma with MOFs catalyst	N_2, O_2	3.3%	2.05	This work

Herein, we use CuBTC and ZIF-8 as the MOF catalysts to assist the atmospheric microwave plasma in nitrogen fixation. These two catalysts can effectively improve nitrogen fixation at different flow rates and microwave power, and the catalytic action is better than the general catalyst ZSM-5.

2. Methods

2.1. Experiment System

Figure 1 shows a photograph of the atmospheric microwave plasma system for nitrogen fixation, which consists of a microwave generator, a circulator (MPWG22CIA01, Mapingtec, Chengdu, China), a water load (MPWG22WLA01, Mapingtec, Chengdu, Sichuan Province, China), a dual-directional coupler (MPWG22CPA01, Mapingtec, Chengdu, Sichuan Province, China), a tapered waveguide, a mass flow controller (MFC, KT-C2Z, Ketanyiqi, Zhengzhou, Henan Province, China), and a Fourier transform infrared (FTIR) spectrometer (Vertex 70, Bruker, Braunschweig, Lower Saxony, Germany). The microwave generator is composed of a water-cooled magnetron (2M265, MUEGGE, Reichelsheim, Hessen, Germany) and a high-voltage DC power supply (Wepex3000BX, Megmeet, Shenzhen, Guangdong Province, China) that drives the magnetron. The magnetron has a center frequency of 2.45 GHz with a maximum output power of 3 kW. The microwave power meter (KC9532, Measall Technology, Chengdu, Sichuan Province, China) is internally built into the microwave generator to detect the incident and reflected microwave powers. Three ports of the circulator are connected to the microwave generator, the coupler, and the water load, respectively. The coupler is connected to the microwave power meter through two coaxial lines to couple the incident and reflected microwave powers for measurement.

A quartz tube with an inner diameter of 25 mm, an outer diameter of 29 mm, and a length of 30 cm was inserted into the tapered waveguide to restrict the plasma. A condenser tube surrounded the quartz tube for cooling. When the plasma was excited, the gas passed through the catalyst and was then detected by the FTIR spectrometer above the quartz tube.

The gas flow rate was adjusted by the MFC which had a range from 1 L/min to 22 L/min. Air was taken as the working gas and it flowed into the quartz tube in the form of a swirl to reduce the heat load of the quartz tube. The concentration of NO_x was obtained by measuring the infrared absorption spectrum of the output gas using the FTIR spectrometer (Vertex 70, Bruker, Braunschweig, Lower Saxony, Germany) locating after the catalyst position. The catalyst was placed in a downstream area which was away from the

plasma torch. This area consisted of reactive oxygen and nitrogen species (RONS), and NO which reacted sufficiently with O_2 to produce NO_2, which can be seen in our measurement results in Section 2.4.

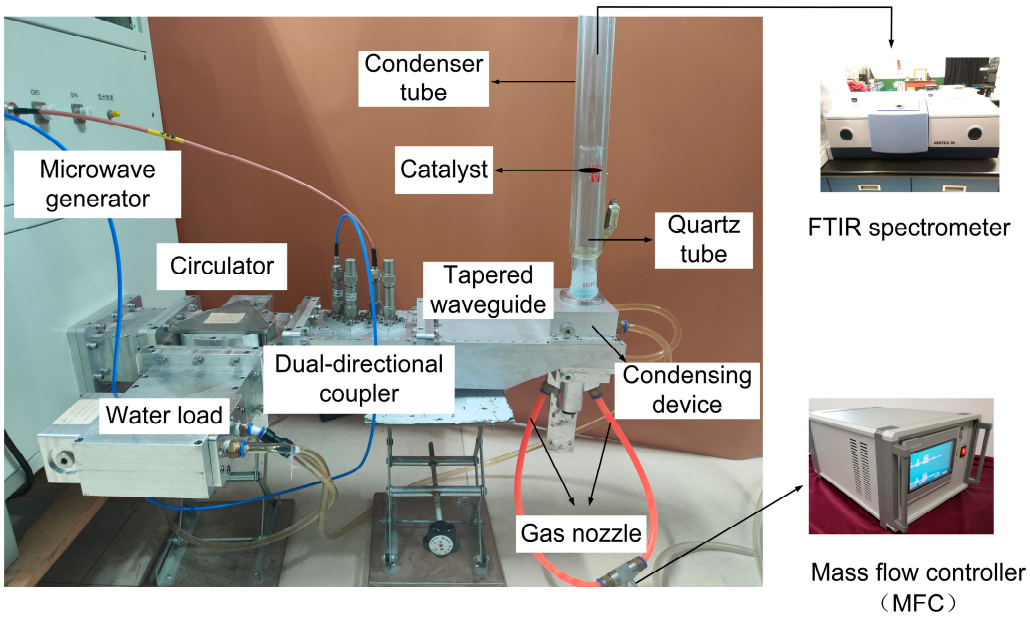

Figure 1. Photograph of the experimental system.

2.2. Catalyst Characterization

In this paper, three catalysts including CuBTC, ZIF-8, and ZSM-5 were used to assist the atmospheric microwave plasma for nitrogen fixation. Both CuBTC and ZIF-8 are MOF materials made by mechanochemical and hydrothermal methods, respectively. ZSM-5 is the zeolite catalyst. All the catalysts were made by the XFNANO Company (Nanjing, China). The MOF catalysts were preheated before each experiment. The weight of catalysts used in each experiment remained at 200 mg. Figure 2 shows pictures of the three catalysts prior to usage.

Figure 2. Photographs of three catalysts prior to usage.

CuBTC is in a light blue powder form, consisting of Cu and benzene-1,3,5-tricarboxylate. It exhibits a regular octahedral crystal structure, characterized by a pore size of 0.9 nm, and a specific surface area of about 457 m^2/g. It needs to be pretreated at 600 °C for three hours before use. ZIF-8 is composed of transition metal ions, zinc, and imidazolate (Im) linkers in a tetrahedral coordination surrounded by nitrogen atoms from the five-membered imidazole ring serving as a bridging linker, i.e., a link connecting the metal centers in the three-dimensional framework. ZIF-8 has a pore size of 0.34~1.16 nm and a specific surface area of about 1345 m^2/g, which needs to be preheated at 1000 °C for ten hours. ZSM-5 is a kind of white powder with a silicon-to-aluminum ratio (SiO_2/Al_2O_3) of 25–30 wt%. The specific surface area is 340 m^2/g and the pore size is about 5 nm.

2.3. Catalyst Location Determination

In this work, the working temperature of both CuBTC and ZIF-8 had to be be below 1000 °C to avoid inactivation [35,36]. However, the gas temperature of the microwave plasma is usually higher than 1000 °C, making it difficult to directly measure this high temperature [39]. Therefore, the temperature distribution of the plasma was simulated to determine a suitable location for placing the catalyst. Moreover, the simulation result is verified by measuring the temperature points below 1000 °C using a digital thermometer. For this measurement, the sensor of the thermometer was placed directly in the specific location of the plasma to obtain the temperature value.

The temperature simulation model was a three-dimensional (3D) domain consisting of a condenser tube, a quartz tube, a condensing device, and a waveguide. Figure 3 shows the *x*-*z* plane of the 3D computational model. Both the condenser tube and condensing device were used to cool the quartz tube when the plasma was generated.

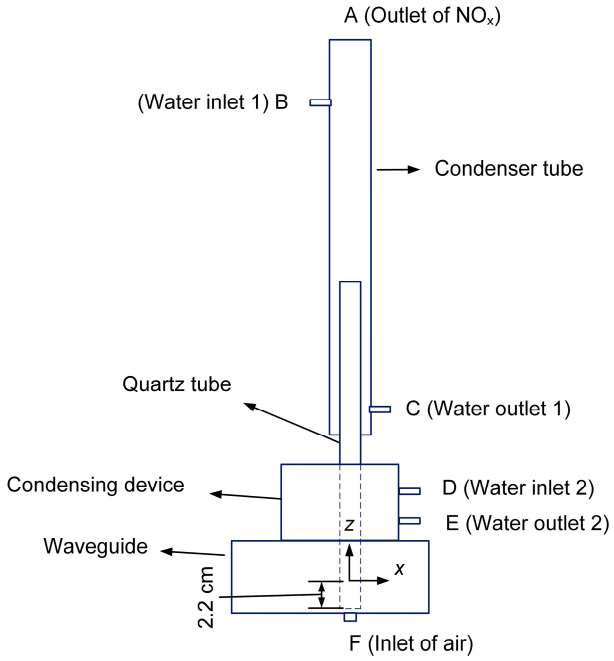

Figure 3. The *x*-*z* plane of the 3D computational model of temperature distribution in plasma and its downstream area.

The working gas flows into the quartz tube from its bottom which is 2.2 cm away from the center of the waveguide. In the simulation, we ignored the swirling form of the inlet gas in front of the quartz tube, and the gas flow in the quartz tube was assumed to be a laminar model. Then, the fluid velocity could be solved using the Navier–Stokes equation [40].

$$\rho(\vec{\boldsymbol{u}} \cdot \nabla)\vec{\boldsymbol{u}} = \nabla \cdot \left[-p\vec{I} + \vec{K}\right] + \vec{F} \quad (1)$$

where ρ is the fluid density with the unit kg/m^3, $\vec{\boldsymbol{u}}$ is the velocity vector of the fluid with the unit m/s, $\rho(\vec{\boldsymbol{u}} \cdot \nabla)\vec{\boldsymbol{u}}$ denotes the net flow of momentum out of a unit volume space, $\left[-p\vec{I} + \vec{K}\right]$ indicates the stress tensor, p is the pressure with the unit Pa, $\vec{K}$ is the viscous stress, and $\vec{F}$ is the external force per unit volume of fluid. Plane F was set as the air inlet and plane A was the gas outlet. For the water flow, planes B and C were set as the inlet and outlet of the condenser tube, while planes D and E were assigned to be the inlet and outlet of the condensing device. The boundaries of the condenser tube, quartz tube, condensing device, and waveguide were all set as the wall boundaries which had velocities of zero .

The gas temperature $\boldsymbol{T}$ is solved by using the heat transfer function [41].

$$\rho C_\rho \vec{\boldsymbol{u}} \cdot \nabla \boldsymbol{T} + \nabla \cdot (-k \nabla \boldsymbol{T}) = Q \quad (2)$$

where C_ρ is the heat capacity with the unit J/(kg·K), k is the thermal conductivity, $\nabla \boldsymbol{T}$ is the temperature gradient, and Q is the heat source. The initial temperature at the plasma core located at the waveguide center is set to be 5300 °C, which is a measured temperature of the atmospheric microwave air plasma [42]. Planes B, D, and F were all used as the inflow boundaries with an initial temperature of 19 °C. The corresponding outflow boundaries were planes C, E, and A, respectively. The outer boundaries of the condenser tube, quartz tube, condensing device, and waveguide were all set to be the convection heat flux q, which is expressed as follows [43].

$$q = h \cdot (\boldsymbol{T}_{ext} - \boldsymbol{T}) \quad (3)$$

where h is the heat transfer coefficient of air with h = 10 W/(m^2·K), and $\boldsymbol{T}_{ext}$ is the temperature of air assumed to be 19 °C. The initial temperature of the simulation domain is also set as 19 °C.

The commercial software COMSOL Multiphysics 5.5 was adopted for the calculations in this paper. The steady-state solver in the software was used to carry out the computation. The convergence criterion of the solver was based on the estimated error and the corresponding tolerance, which was set to 0.001. The convergence was reached when the estimated error was smaller than the corresponding tolerance. Figure 4a,b illustrate the grid diagram used in our simulation and the grid sensitivity test. Seven sets of grids with different grid numbers were plotted for the model in the sensitivity test. When the grid number surpasses 434,499, the average temperature will reach a stable state. Free tetrahedral grids with the maximum and minimum sizes of 13 mm and 0.13 mm, respectively, were generated for the simulation domain. The total grid number is 873,403 with 86,641 unknowns. All the computations were calculated using a workstation with an Intel(R) Xeon(R) E5-2650 CPU at 2.3 GHz and a RAM of 96 GB based on the 64-bit Windows10 platform (Intel Corporation, Santa Clara, CA, USA).

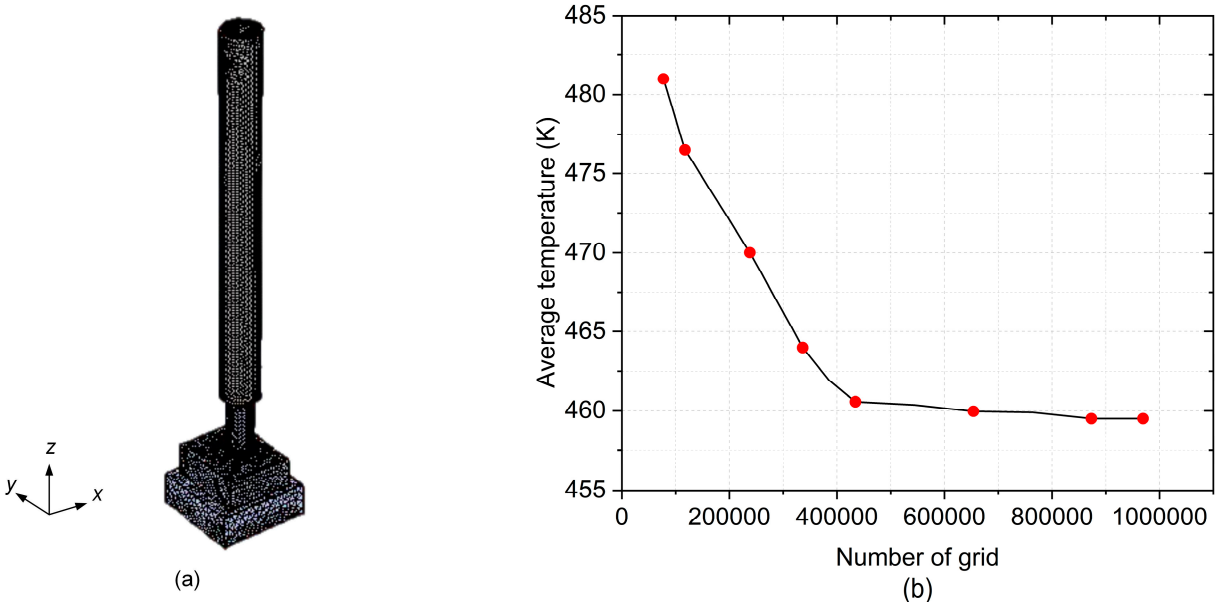

Figure 4. (**a**) Mesh diagram used in the simulation, and (**b**) the mesh sensitivity test.

A diagram depicting the simulated 3D temperature distribution is presented in Figure 5a. It is clear that the gas temperature in the quartz tube decreases gradually with the direction of airflow. The condensing equipment has a significant effect on cooling the quartz tube as the temperature inside the quartz tube in the waveguide is significantly

higher than that in other areas of the waveguide. It can be seen from Figure 5c that the temperature distribution in the *x*-*y* cross section of the quartz tube exhibits a divergent pattern with a high central temperature and a low edge temperature. Figure 6 shows the specific temperature values of the points on the *z*-axis. As z increases, the temperature will decrease. According to Figure 6, the gas temperature will be below 1000 °C when z is greater than 18 cm. Therefore, we measured the temperature values at *z* = 19.7, 20, 29, 40.5, and 50 cm, which are shown as the red points in Figure 6. The measured temperatures are in good agreement with the simulation results. As the catalysts used in this paper can work at 600 °C [35,36], the location of *z* = 24 cm with a maximum temperature of 600 °C was selected as the catalyst position. Moreover, the streamline chart of the laminar flow at an inflow rate of 7 L/min is shown in Figure 7. Due to the fact that the gas inlet of our simulation model was parallel to the *z*-axis, the gas flow rate decreased with the *z*-axis.

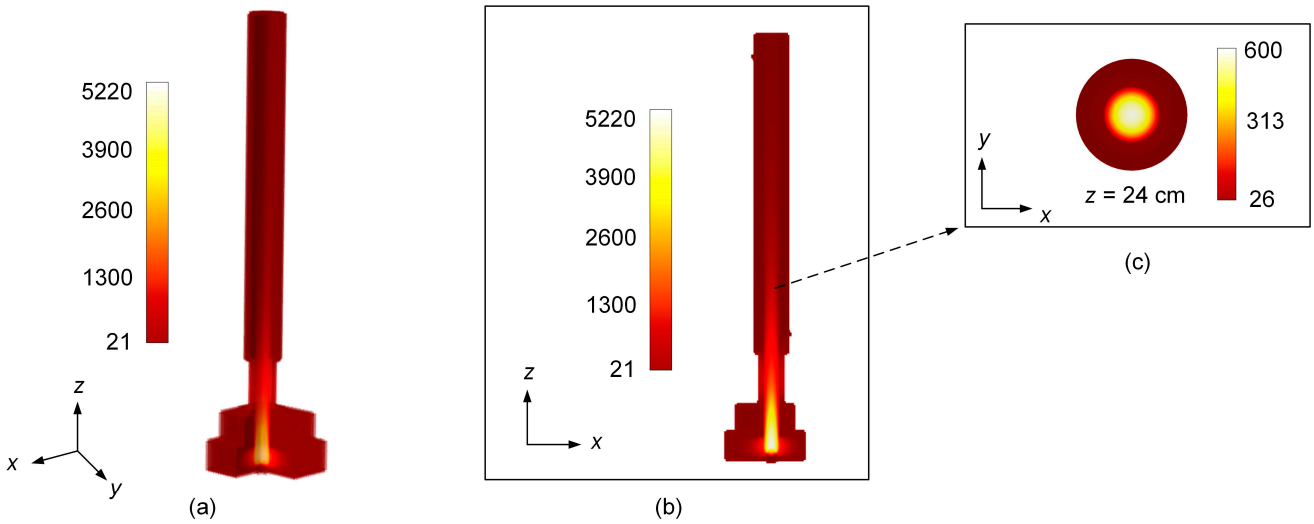

Figure 5. Temperature distribution in (**a**) 3D model, (**b**) *x*-*z* plane and (**c**) *x*-*y* plane (unit: °C).

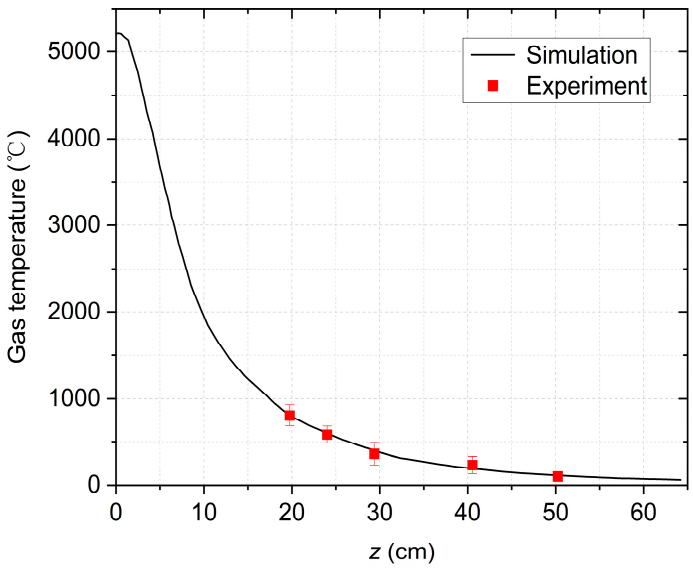

Figure 6. Gas temperature at the *z*-axis in the quartz tube.

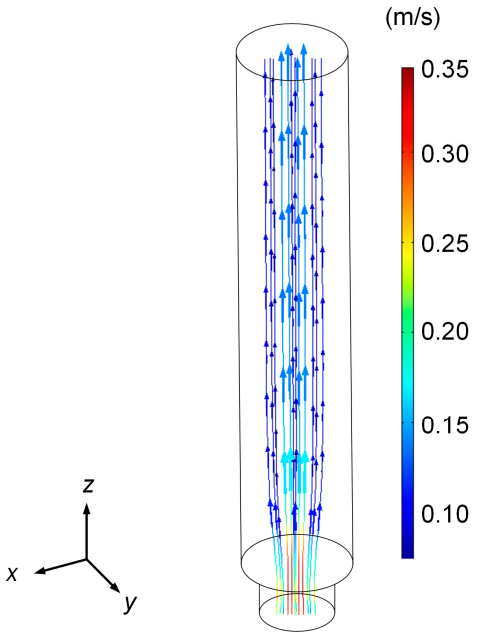

Figure 7. The streamline chart for the inflow rate 7 L/min.

2.4. NO_x Measurement

The infrared absorption spectra of the gasses generated by microwave plasma in different conditions were detected to determine the NO_x concentrations. Figure 8 shows the spectra at the gas flow rates of 9 L/min and the microwave power of 450 W. It can be observed that NO_x mainly consists of NO_2 and NO [18]. Moreover, the concentration of NO_2 is much higher than that of NO since most of the NO will react with the oxidative species to produce NO_2 in the measurement area. Thus, the total concentrations of NO_2 and NO were determined using the NO_x concentrations in this paper.

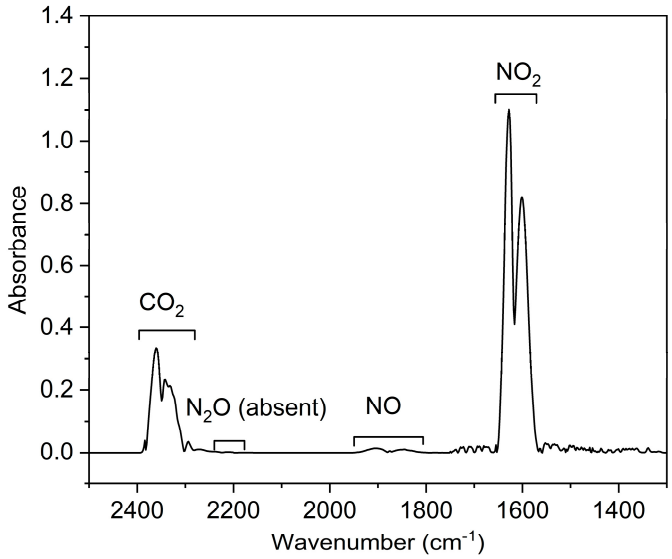

Figure 8. Infrared absorption spectrum of the gas generated using the atmospheric microwave plasma.

Figure 9a,c show the infrared absorption spectra of NO and NO_2 with standard concentrations measured by FTIR. According to the absorption peaks at 1905 cm^{-1} for NO and 1627.8 cm^{-1} for NO_2 [18], the calibration curves for NO and NO_2 were built as

shown in Figure 9b,d to determine their concentrations. The relationship between the concentration and absorbance of these two curves is approximately linear.

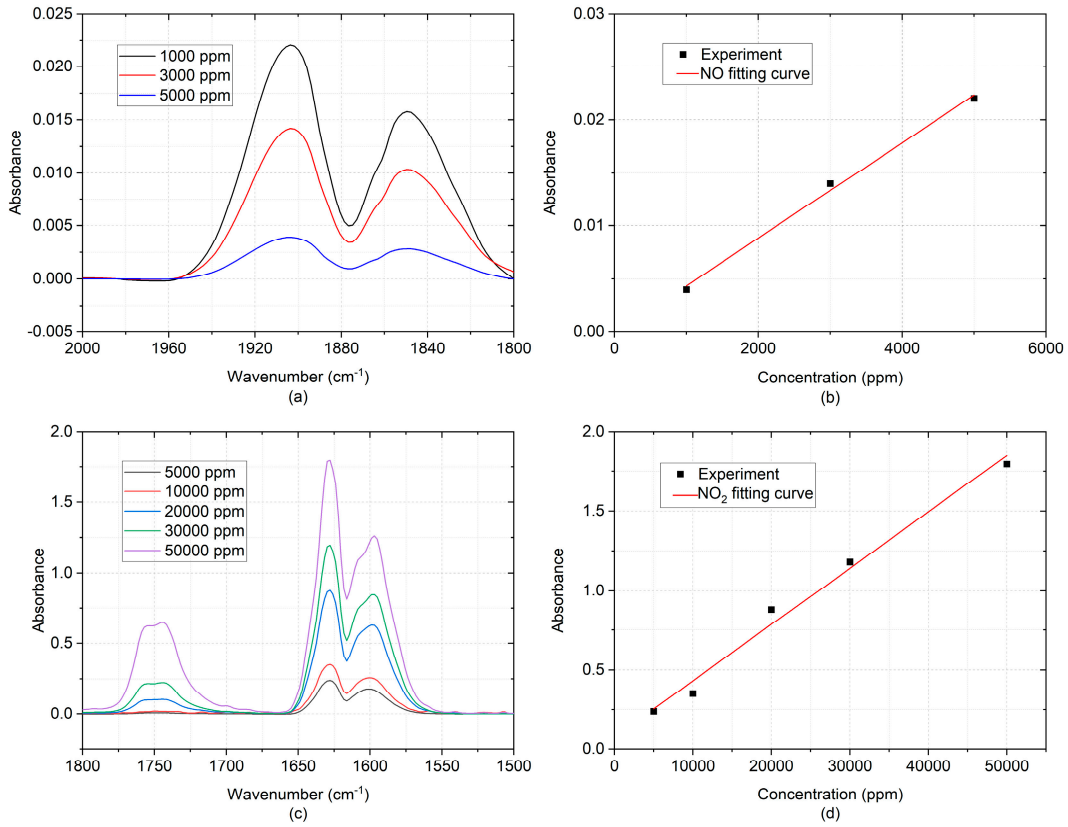

Figure 9. Infrared absorption spectra of (**a**) NO and (**c**) NO_2 with standard concentrations and the calibration curves of (**b**) NO and (**d**) NO_2.

The energy consumption was calculated using the following formula,

$$E_{NO_x} = \frac{P \cdot L_m \cdot 60[\mathrm{s/min}]}{C_{NO_x} \cdot f_l} \quad (4)$$

where E_{NO_x} is the energy consumption with the unit MJ/mol, P represents the microwave power, L_m is the molar volume of ideal gas at atmospheric pressure and room temperature which is equal to 24.05 L/mol, C_{NO_x} is the NO_x concentration with the unit ppm (parts per million), and f_l is the gas flow rate with the unit L/min.

3. Experiment Results and Discussions

In the experiment, three different catalysts were placed in the same positions determined in Section 2.3, and the nickel foam was fixed there as the catalyst carrier due to its cheapness and high temperature resistance. The blank group indicates no nickel foam and catalyst packed downstream of the microwave plasma, and the nickel foam group which had no catalyst is taken as the control group. Plasma cannot be generated when the microwave power falls below 400 W. When the microwave power exceeds 750 W, the plasma temperature rises excessively, potentially compromising the catalytic efficiency of MOFs. Hence, we opted for a microwave power range of 450 W to 700 W. Then, the NO_x concentration and energy consumption could be obtained at different microwave power and gas flow rates.

3.1. NO_x Production

Figure 10 shows the NO_x concentrations with gas flow rates ranging from 3 L/min to 13 L/min at four different microwave powers. The NO_x concentration in the blank group is similar to that in the control group, which indicates that the nickel foam has little effect on the production of NO_x. The NO_x concentrations are higher in the three catalysts than in the control group, showing that three catalysts can promote the synthesis of NO_x. Among these catalysts, CuBTC and ZIF-8 have higher NO_x concentrations than ZSM-5.

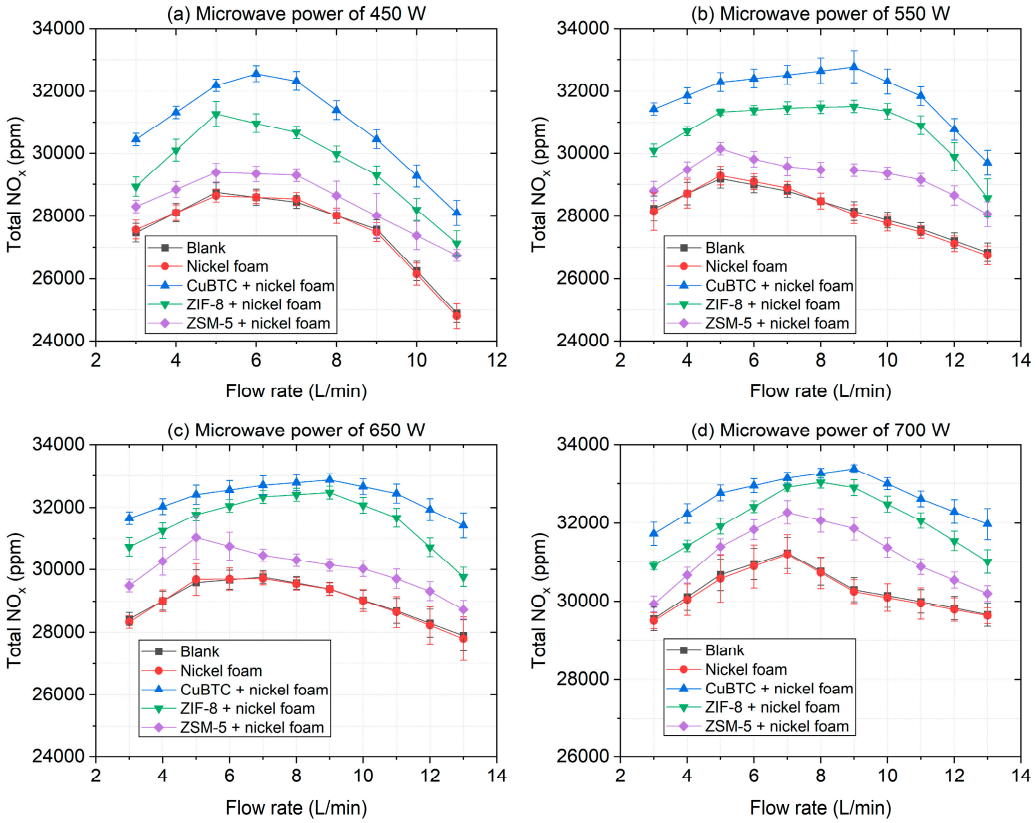

Figure 10. NO_x concentration at different gas flow rates and microwave powers of (**a**) 450 W, (**b**) 550 W, (**c**) 650 W, and (**d**) 700 W.

As the microwave power remains constant, the NO_x concentration firstly increases and then decreases with the increment in the gas flow rate. This is consistent with the trend of the visible length of the plasma changing with the gas flow rate [42]. When the gas flow rate is 3 L/min, the plasma torch is short, leading to a small reaction area. As the gas flow rate slowly increases from 3 L/min to a medium flow rate within the range of 7 L/min to 9 L/min, the length of the plasma torch increases, which results in a bigger reaction area for NO_x synthesis. When the gas flow rate is too high, the propagation distance of the surface wave that maintains the plasma becomes short, causing a decrement in the plasma torch length [44]. Moreover, the gas residence time also becomes smaller at high gas flow rates; hence, the NO_x concentration is rapidly reduced. When the microwave power increases from 450 W to 700 W, the gas flow rate corresponding to the maximum NO_x concentration increases from 5 L/min to 9 L/min. When the gas flow rate remains constant, the NO_x concentration increases as the microwave power increases due to the increment in the specific energy input (SEI), which is shown in Equation (5) [12]. As the energy gained per unit volume of gas increases, more N_2 and O_2 will participate in the reaction, thus increasing the NO_x concentration.

$$SEI = \frac{P(\mathrm{W})}{f_l(\mathrm{L/min})} \quad (5)$$

When the microwave power was 700 W and the flow rate was 9 L/min with CuBTC, the maximum NO_x concentration of 33,400 ppm in the experiment was obtained. Comparing the results of CuBTC and the blank group, it can be seen that the NO_x concentration can be increased from 28,000 ppm to 32,800 ppm with a maximum increment of 17.1% under the conditions of 9 L/min and 550 W.

3.2. Energy Consumption

Figure 11 shows the energy consumption of the nitrogen fixation reaction under the same conditions as shown in Figure 10. It was found that three catalysts can decrease the energy consumption of nitrogen fixation. As the gas flow rate increases while the microwave power remains constant, the energy consumption decreases. According to Equation (4), the energy consumption is inversely proportional to the NO_x concentration and gas flow rate, and directly proportional to the microwave power. When the microwave power remains constant and the gas flow rate increases from 3 to 5 L/min, the energy consumption decreases rapidly because the NO_x concentration increases with the gas flow rate. When the gas flow rate increases gradually from 5 L/min to a medium flow rate (7 to 9 L/min), the energy consumption decreases slowly due to the slow increment or even decrement in the NO_x concentration. When the microwave power is at high levels such as 650 W and 700 W, and the gas also flows at high rates of 11 and 13 L/min, the energy consumption almost levels off due to the very rapid decrement in the NO_x concentration.

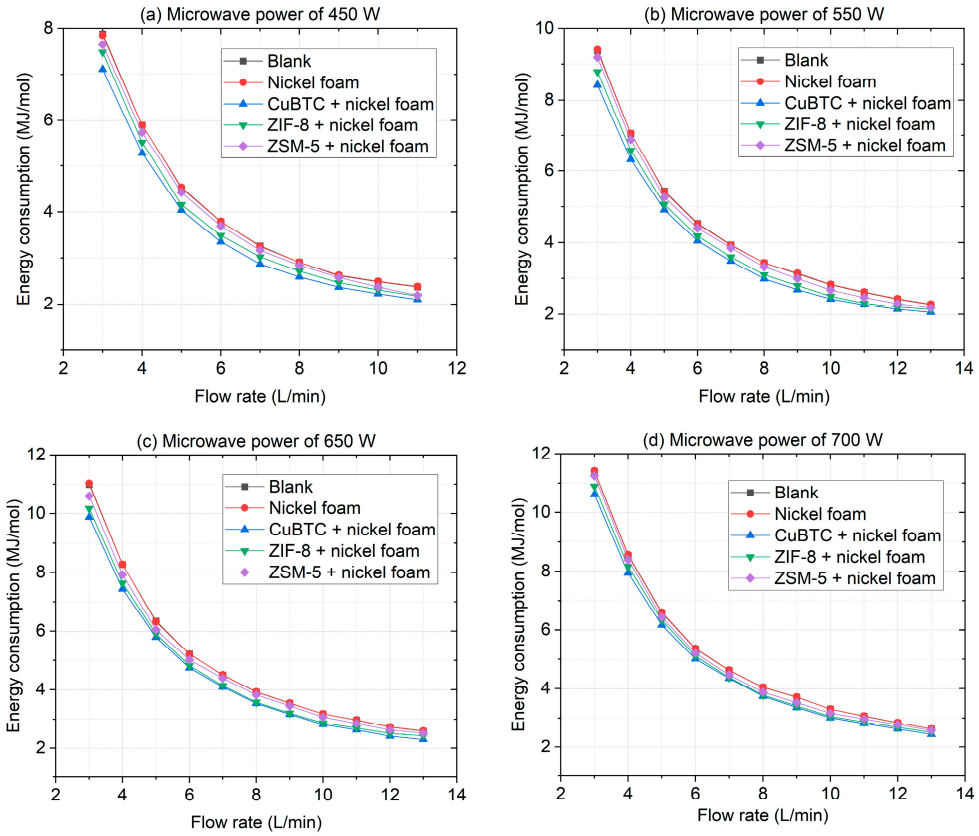

Figure 11. Energy consumption with different gas flow rates and microwave powers of (**a**) 450 W, (**b**) 550 W, (**c**) 650 W, and (**d**) 700 W.

At different microwave power and gas flow rates, the energy consumption using ZSM-5 was higher than that with CuBTC and ZIF-8. The minimum energy consumption obtained in the experiment was 2.05 MJ/mol, which was reduced by 10.1% compared to no catalyst. This was achieved by using CuBTC as the catalyst at a microwave power of 550 W and a gas flow rate of 13 L/min. Compared to the results of the blank group, the energy

consumption in the experiment is reduced maximally by 14.6% using CuBTC at 9 L/min and 550 W.

3.3. Stability Test of the Catalysts

In order to study the stability of the catalysts, plasma-based nitrogen fixation experiments are conducted on three catalysts at different gas flow rates and microwave powers within one hour. Figure 12 shows the changes in the NO_x concentration produced using these three catalysts during a 60 min operation. Within the four sets of microwave power and gas flow rates, there is little change in the NO_x concentration using three catalysts, which indicates that the catalyst activity remained stable over this period.

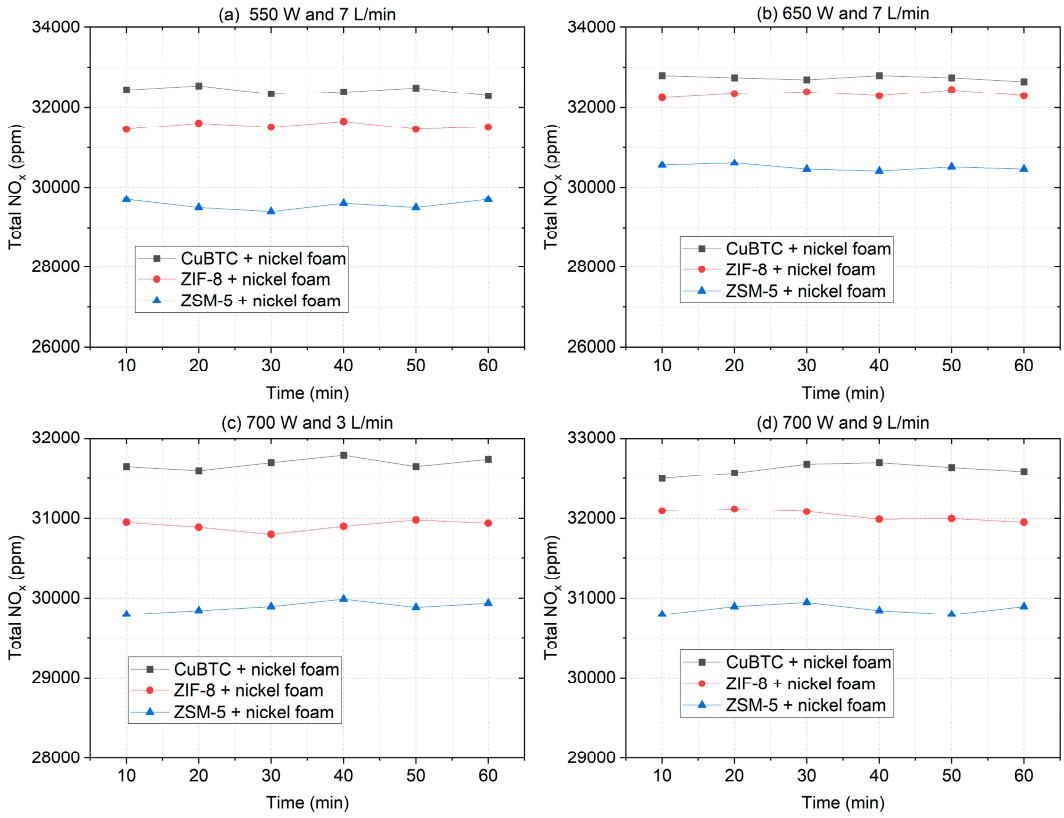

Figure 12. NO_x concentration produced during a 60 min operation with these three catalysts.

4. Conclusions

In this paper, the effect of MOF materials on nitrogen fixation by microwave plasma at atmospheric pressure was investigated. The experimental results show that the MOF materials of CuBTC and ZIF-8 can effectively increase NO_x production and reduce energy consumption at different microwave powers and gas flow rates, and the improvement surpasses the results with the general catalyst ZSM-5. The maximum NO_x concentration obtained in the experiment reached 33,400 ppm and the minimum energy consumption was 2.05 MJ/mol. Compared to the results without the catalyst, the energy consumption was reduced by 14.6% and the NO_x production was increased by 17.1%. In addition, the three catalysts provided a stable performance within one hour. This paper verifies the superiority of combining atmospheric microwave plasma with MOF catalysts for nitrogen fixation, benefiting the industrial promotion of plasma-based nitrogen fixation technology.

Author Contributions: Conceptualization, W.X.; methodology, F.Z.; software, F.Z.; validation, S.W.; formal analysis, K.F. and S.W.; investigation, K.F.; resources, F.Z.; data curation, K.F. and S.W.; writing—original draft preparation, F.Z.; writing—review and editing, W.X.; visualization, F.Z.; supervision, W.X.; project administration, W.X.; funding acquisition, W.X. All authors have read and agreed to the published version of the manuscript.

Funding: This research was funded by the National Natural Science Foundation of China under grant number 62101146 and the Guizhou University Talent Project under grant number 2020-51.

Data Availability Statement: The original contributions presented in the study are included in the article, further inquiries can be directed to the corresponding author.

Conflicts of Interest: The authors declare no conflicts of interest.

References

1. Galloway, N.J.; Cowling, B.E. Reactive Nitrogen and The World: 200 Years of Change. *AMBIO* **2022**, *31*, 64–71. [CrossRef] [PubMed]
2. Winter, L.R.; Chen, J.G. N_2 Fixation by Plasma-Activated Processes. *Joule* **2020**, *5*, 300–315. [CrossRef]
3. Wilson, A.; Staack, D.; Farouk, T.; Gutsol, A.; Fridman, A.; Farouk, B. Self-rotating dc atmospheric-pressure discharge over a water-surface electrode: Regimes of operation. *Plasma Sources Sci. Technol.* **2008**, *17*, 45001. [CrossRef]
4. Chanway, C.P.; Anand, R.; Yang, H. Nitrogen Fixation Outside and Inside Plant Tissues. In *Advances in Biology and Ecology of Nitrogen Fixation*; IntechOpen: Rijeka, Croatia, 2014; pp. 3–21. [CrossRef]
5. Bond, D.W.; Steiger, S.; Zhang, R.; Tie, X.; Orville, R.E. The importance of NO_x production by lightning in the tropics. *Orville. Atmos. Environ.* **2002**, *36*, 1509–1519. [CrossRef]
6. Patil, B.S.; Wang, Q.; Hessel, V.; Lang, J. Plasma N_2-fixation: 1900–2014. *Catal. Today.* **2015**, *256*, 49–66. [CrossRef]
7. Zhang, J.; Li, X.; Zheng, J. Non-thermal plasma-assisted ammonia production: A review. *Energy Convers. Manag.* **2023**, *293*, 117482. [CrossRef]
8. Li, L.; Tang, C.; Jin, H.; Davey, K.; Qiao, S.Z. Main-group elements boost electrochemical nitrogen fixation. *Chem* **2021**, *7*, 3232–3255. [CrossRef]
9. Wang, W.; Qu, J.; Li, C.; Guo, L.; Fang, X.; Chen, G. "MoFe cofactor" inspired iron mesh-based MIL-88A(Fe/Mo) for bionic photocatalytic nitrogen fixation. *Mol. Catal.* **2022**, *532*, 112730. [CrossRef]
10. Tsone, I.; O'Modhrai, C.; Bogaerts, A.; Gorbanev, Y. Nitrogen Fixation by an Arc Plasma at Elevated Pressure to Increase the Energy Efficiency and Production Rate of NO_x. *ACS Sustain. Chem. Eng.* **2023**, *11*, 1888–1897. [CrossRef]
11. Pei, X.; Gidon, D.; Yang, Y.-J.; Xiong, Z.; Graves, D.B. Reducing energy cost of NO_x production in air plasmas. *Chem. Eng. J.* **2019**, *362*, 217–228. [CrossRef]
12. Patil, B.S.; Cherkasov, N.; Lang, J.; Ibhadon, A.O.; Hessel, V.; Wang, Q. Low temperature plasma-catalytic NO_x synthesis in a packed DBD reactor: Effect of support materials and supported active metal oxides. *Appl. Catal. B.* **2016**, *194*, 123–133. [CrossRef]
13. Vervloessem, E.; Gorbanev, Y.; Nikiforov, A.; Geyter, N.D.; Bogaerts, A. Sustainable NOx production from air in pulsed plasma: Elucidating the chemistry behind the low energy consumption. *Green Chem.* **2022**, *24*, 916–929. [CrossRef]
14. Iqbal, M.; Hoon, L.D.; Khoe, D.D. A novel energy efficient path for nitrogen fixation using a non-thermal arc. *RSC Adv.* **2021**, *11*, 12729–12738. [CrossRef]
15. Vervloessem, E.; Aghaei, M.; Jardali, F.; Hafezkhiabani, N.; Bogaerts, A. Plasma-Based N_2 Fixation into NO_x: Insights from Modeling toward Optimum Yields and Energy Costs in a Gliding Arc Plasmatron. *ACS Sustain. Chem. Eng.* **2020**, *8*, 9711–9720. [CrossRef]
16. Lei, X.Y.; Cheng, H.; Nie, L.L.; Lu, X.P. Nitrogen Fixation as NO_x Enabled by a Three-Level Coupled Rotating Electrodes Air Plasma at Atmospheric Pressure. *Plasma Chem. Plasma Process.* **2022**, *42*, 211–227. [CrossRef]
17. Malik, M.A.; Jiang, C.; Heller, R.; Lane, J.; Hughes, D.; Schoenbach, K.H. Ozone-free nitric oxide production using an atmospheric pressure surface discharge—A way to minimize nitrogen dioxide co-production. *Chem. Eng. J.* **2016**, *283*, 631–638. [CrossRef]
18. Bahnamiri, O.S.; Verheyen, C.; Snyders, R.; Bogaerts, A.; Britun, N. Nitrogen fixation in pulsed microwave discharge studied by infrared absorption combined with modelling. *Plasma Sources Sci. Technol.* **2021**, *30*, 065007. [CrossRef]
19. Mutel, B.; Dessaux, O.; Goudmand, P. Energy cost improvement of the nitrogen oxides synthesis in a low pressure plasma. *Rev. Phys. Appl.* **1984**, *19*, 461–464. [CrossRef]
20. Seán, K.; Annemie, B. Nitrogen fixation in an electrode-free microwave plasma. *Joule* **2021**, *5*, 3006–3030. [CrossRef]
21. Patil, B.S.; Palau, J.R.; Hessel, V.; Lang, J.; Wang, Q. Plasma Nitrogen Oxides Synthesis in a Milli-Scale Gliding Arc Reactor: Investigating the Electrical and Process Parameters. *Plasma Chem. Plasma Process.* **2016**, *36*, 241–257. [CrossRef]
22. Asisov, R.I.; Givotov, V.K.; Rusanov, V.D.; Fridman, A. Spin effects in elementary processes of high-energy chemistry. *Khim. Vys. Energ.* **1980**, *14*, 366.
23. Rouwenhorst, K.H.R.; Jardali, F.; Bogaerts, A.; Lefferts, L. From the Birkeland-Eyde process towards energy-efficient plasma-based NO_x synthesis: A techno-economic analysis. *Energy Environ. Sci.* **2023**, *16*, 6170–6173. [CrossRef] [PubMed]

24. Peng, P.; Schiappacasse, C.; Zhou, N. Sustainable Non-Thermal Plasma-Assisted Nitrogen Fixation—Synergistic Catalysis. *ChemSusChem* **2019**, *12*, 3702–3712. [CrossRef] [PubMed]
25. Hollevoet, L.; Vervloessem, E.; Gorbanev, Y. Energy-Efficient Small-Scale Ammonia Synthesis Process with Plasma-Enabled Nitrogen Oxidation and Catalytic Reduction of Adsorbed NO_x. *ChemSusChem* **2022**, *15*, e202102526. [CrossRef] [PubMed]
26. Pei, X.I.; Li, Y.; Luo, Y. Nitrogen fixation as NO_x using air plasma coupled with heterogeneous catalysis at atmospheric pressure. *Plasma Process. Polym.* **2023**, *21*, e2300135. [CrossRef]
27. Zhang, B.; Li, J.; Zuo, H.; Kamiya, K.; Chen, Y.; Chen, G. Reinforcement of fluidized catalysts with dbd plasma assisted for green ammonia synthesis. *Int. J. Hydrogen Energy.* **2024**, *67*, 521–531. [CrossRef]
28. Nguyen, H.M.; Omidkar, A.; Li, W.; Meng, S.; Li, Z.; Song, H. Non-thermal plasma assisted catalytic nitrogen fixation with methane at ambient conditions. *Chem. Eng. J.* **2023**, *471*, 144748. [CrossRef]
29. Javishk, S.; Ting, W.; Jolie, L.; Moises, A.C.; Maria, C.L. Nonthermal Plasma Synthesis of Ammonia over Ni-MOF-74. *ACS Sustain. Chem. Eng.* **2019**, *7*, 377–383. [CrossRef]
30. Wandell, R.J.; Wang, H.H.; Bulusu, R.K.M.; Gallan, R.O.; Locke, B.R. Formation of nitrogen oxides by nanosecond pulsed plasma discharges in gas-liquid reactors. *Plasma Chem. Plasma Process.* **2019**, *39*, 643–666. [CrossRef]
31. Liu, Y.; Wang, C.W.; Xu, X.F. Synergistic effect of Co-Ni bimetal on plasma catalytic ammonia synthesis. *Plasma Chem. Plasma Process.* **2022**, *42*, 267–282. [CrossRef]
32. Gorky, F.; Lucero, J.M.; Crawford, J.M.; Blake, B.; Carreon, M.A.; Carreon, M.L. Plasma-induced catalytic conversion of nitrogen and hydrogen to ammonia over zeolitic imidazolate frameworks ZIF-8 and ZIF-67. *ACS Appl. Mater. Interfaces* **2021**, *13*, 21338–21348. [CrossRef] [PubMed]
33. Shah, J.; Wang, W.; Bogaerts, A.; Carreon, M.L. Ammonia synthesis by radio frequency plasma catalysis: Revealing the underlying mechanisms. *ACS Appl. Energy Mater.* **2018**, *1*, 4824–4839. [CrossRef]
34. Farha, O.K.; Eryazici, I.; Jeong, N.C. Metal−organic framework materials with ultrahigh surface areas: Is the sky the limit? *J. Am. Chem. Soc.* **2012**, *134*, 15016–15021. [CrossRef] [PubMed]
35. Zhang, L.J.; Su, Z.X.; Jiang, F.L. Highly graphitized nitrogen-doped porous carbon nanopolyhedra derived from ZIF-8 nanocrystals as efficient electrocatalysts for oxygen reduction reactions. *Nanoscale* **2014**, *6*, 6590. [CrossRef] [PubMed]
36. Jalal, A.; Zhao, Y.; Uzun, A. Pyrolysis temperature tunes the catalytic properties of cubtc-derived carbon-embedded copper catalysts for partial hydrogenation. *Ind. Eng. Chem. Res.* **2022**, *61*, 2068–2080. [CrossRef]
37. Wu, G.; Ma, J.; Li, S. Cationic metal-organic frameworks as an efficient adsorbent for the removal of 2,4-dichlorophenoxyacetic acid from aqueous solutions. *Environ. Res.* **2020**, *186*, 109542. [CrossRef]
38. Wei, Q.X.; Shan, H.; Sheng, J.L. Post-synthetic modification of a metal-organic framework based on 5-aminoisophthalic acid for mercury sorption. *Inorg. Chem. Commun.* **2019**, *108*, 107515. [CrossRef]
39. Huang, S.; Liu, C.; Jie, Z.; Zhang, G. Imaging Diagnostics and Gas Temperature Measurements of Atmospheric-Microwave-Induced Air Plasma Torch. *IEEE Trans. Plasma Sci.* **2020**, *48*, 2958. [CrossRef]
40. Ivorra, B. Application of the Laminar Navier–Stokes Equations for Solving 2D and 3D Pathfinding Problems with Static and Dynamic Spatial Constraints: Implementation and Validation in Comsol Multiphysics. *J. Sci. Comput.* **2018**, *74*, 1163–1187. [CrossRef]
41. Wei, X.; Huang, K.; Zhang, W.; Yi, L. Modeling of Argon Plasma Excited by Microwave at Atmospheric Pressure in Ridged Waveguide. *IEEE Trans. Plasma Sci.* **2016**, *44*, 1075–1082. [CrossRef]
42. Xiao, W.; Liao, Y.; Wang, F. Determining Electron Density of Atmospheric Microwave Air Plasma Torch by Microwave Power Measurement. *IEEE Trans. Plasma Sci.* **2022**, *50*, 1781–1789. [CrossRef]
43. Pitchai, K.; Chen, J.; Birla, S.; Gonzalez, R.; Jones, D.; Subbiah, J. A microwave heat transfer model for a rotating multi-component meal in a domestic oven: Development and validation. *Food Eng.* **2014**, *128*, 60–71. [CrossRef]
44. Zhang, W.; Wu, L.; Tao, J.; Huang, K. Numerical Investigation of the Gas Flow Effects on Surface Wave Propagation and Discharge Properties in a Microwave Plasma Torch. *IEEE Trans. Plasma Sci.* **2019**, *47*, 271–277. [CrossRef]